NASA TM X-1557

EFFECT OF FINNED-TUBE ASSEMBLY TECHNIQUES ON THE HEAT-TRANSFER CHARACTERISTICS OF A SPACE RADIATOR

By Lawrence A. Mueller

Lewis Research Center
Cleveland, Ohio

NATIONAL AERONAUTICS AND SPACE ADMINISTRATION

For sale by the Clearinghouse for Federal Scientific and Technical Information
Springfield, Virginia 22151 – CFSTI price $3.00

EFFECT OF FINNED-TUBE ASSEMBLY TECHNIQUES ON THE HEAT-TRANSFER CHARACTERISTICS OF A SPACE RADIATOR

by Lawrence A. Mueller

SUMMARY

Nine methods of fabricating a finned-tube space radiator were tested. Both mechanical and metallurgical joining of stainless-steel tubes to aluminum meteoroid armor and fins were investigated and compared with an all-aluminum radiator. The mechanically assembled sample had a heat-radiating capacity of 125 to 236 watts per foot of tube length (410 to 774 W/m), and the metallurgically assembled samples radiated 231 to 287 watts per foot (758 to 941 W/m). A brazed assembly had the best heat-transfer characteristics. Measured thermal resistance ranged from 0.07 to 1.5 (^{o}F)(ft)/W (0.011 to 0.258 (^{o}K)(m)/W). Also, the metallurgically joined specimens were not affected by thermal cycling; whereas, all the mechanically assembled specimens, except the bumper finned-tube sample, were affected.

INTRODUCTION

Space radiators are used to reject waste heat from various spacecraft power generating systems. A typical radiator is one that is constructed of a number of parallel finned tubes (ref. 1). The waste heat is transferred from the power generating system to the finned-tube radiator by means of a working fluid (liquid metal, organic fluid, etc.). The fins on the tubes dissipate the heat by radiating to the space heat sink.

When compatibility between the working fluid and the conveying tubes is a problem, it usually becomes necessary to fabricate the radiator from two dissimilar metals. Stainless steel might be selected for the tubes since it is compatible with most fluids and has high strength at elevated temperatures. A material which is light weight and has good heat conduction and meteoroid protection properties, such as aluminum, might be selected for the armor and fins.

The use of these materials presents a problem since they must be joined in a manner that produces good heat-transfer characteristics. In order to achieve this, intimate contact between the two materials is extremely important.

For this reason nine different techniques of bimetal joining were investigated and are explained in this report. Both mechanical and metallurgical fabrication techniques were used. All finned-tube assemblies were evaluated by testing at space-simulating pressure and heat-sink temperature. With these data the reader can compare design and fabrication simplicity with heat-transfer effectiveness and efficiency. The heat-rejection temperature used in the evaluation was 700° F (644° K), and the heat-sink temperature was -320° F (78° K).

DESCRIPTION OF FINNED-TUBE RADIATOR ASSEMBLIES

Nine different methods were investigated for attaching aluminum armor and fins to stainless-steel tubes. These assemblies represented manufacturing techniques of welding, brazing, casting, and metal forming. Figure 1 is a photograph of a typical assembly showing pertinent details.

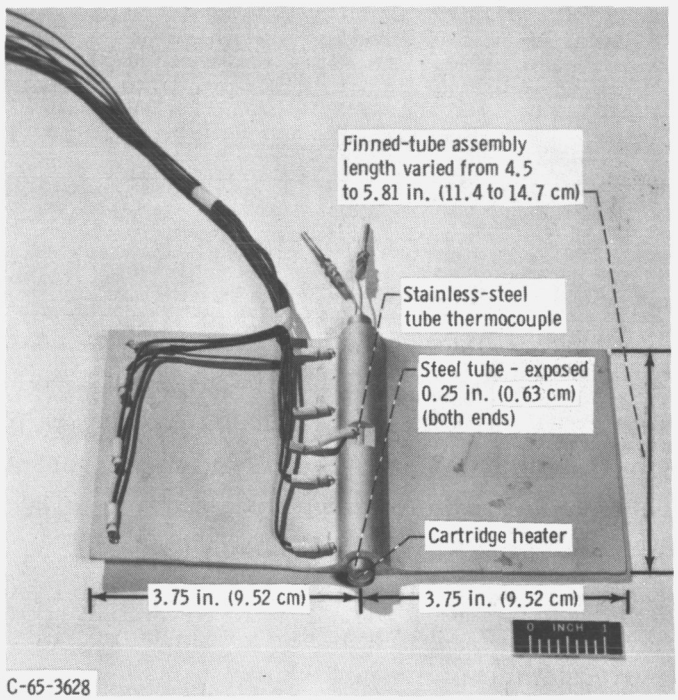

Figure 1. - Typical finned-tube assembly.

Figure 2 shows the details of the finned-tube assembly of each configuration. As a reference for the tests, a finned-tube was machined from an aluminum plate, (fig. 2(a)) to the same dimensions as the aluminum to stainless-steel finned-tube assemblies. This all-aluminum reference sample has the heater fitted directly in contact with the aluminum tube wall; there was no stainless-steel insert in the assembly. A thermocouple was embedded 0.030-inch (0.076-cm) deep into the aluminum tube to measure a simulated stainless-steel tube temperature at the same location as in the other finned-tube assemblies.

Three assemblies (samples B, C, and D) represented metallurgical bonding fabrication techniques. Aluminum brazing alloy (aluminum - 12.0 silicon - 0.30 copper - 0.08 iron - 0.20 zinc - 0.10 magnesium - 0.15 manganese) was used to braze the fin to the stainless-steel tube of samples B and C. Excess braze material on sample B was machined away to give a symmetrical shape of an approximately 0.09-inch (0.228-cm) thickness and an 0.09-inch (0.228-cm) radius.

Samples E to H represented machined shapes that could be formed by an extrusion process but mechanically attached to the stainless-steel tube. The bumper sections on sample E (fig. 2(e)) were made from 0.875-inch (2.222-cm) outside diameter by 0.187-inch (0.474-cm) wall aluminum pipe. A sector of approximately 135° was cut from a pipe and then the balance of the pipe was machined to fit over the 0.03-inch aluminum sheath.

APPARATUS AND PROCEDURE

The tests on the heat-transfer characteristics of the bimetallic assemblies were conducted in an 18-inch (46-cm) diameter vacuum bell jar (fig. 3). A cold-wall heat sink was fabricated from an 8- by 16-inch (20- by 41-cm) copper plate that had a copper tube brazed to the rear surface for liquid-nitrogen cooling. The front side of the cold wall was painted flat black to increase its thermal absorptivity. All coolant and electrical connections were brought out through a stainless-steel spool section under the bell jar.

Each finned-tube test assembly was heated by a cartridge resistance heating element inserted into each finned tube. The outside diameter of the heating element was so machined and polished that it would lightly slip into the tube of each assembly. The heating element and finned tube were then installed in the vacuum bell jar for testing. The assembly was supported by an insulating block to reduce conductive heat transfer. A schematic of the instrumented assembly, vertically mounted and facing the liquid-nitrogen-cooled heat sink, is shown in figure 3. Figure 4 shows the test facility, instrumented assembly, and support equipment. To restrict heating of the glass dome of the bell jar from thermal radiation of the assembly, a polished stainless-steel reflecting

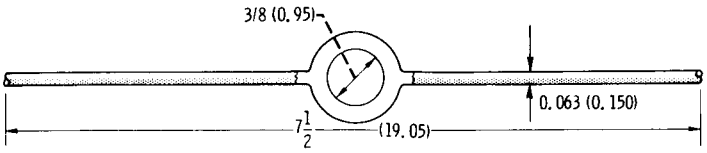

(a) Sample A, all aluminum reference fin. Machined from 1100° aluminum plate.

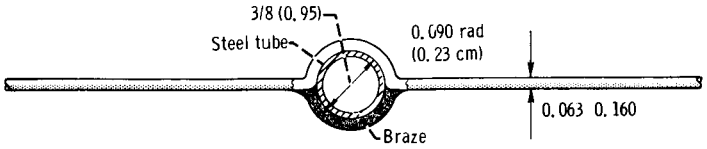

(b) Sample B. Fins formed from 3003 aluminum and brazed to 0.375-inch (0.92-cm) outside diameter by 0.015-inch (0.038-cm) wall. AISI 316 stainless-steel tube.

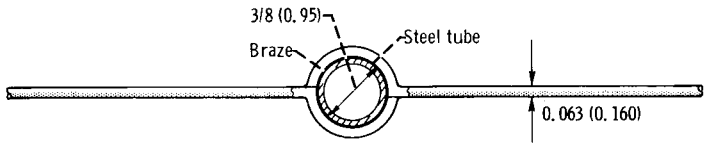

(c) Sample C. Fin halves formed from 3003 aluminum. Each half encompasses 180° of stainless-steel tube. Components brazed together. AISI stainless-steel tube dimensions, 0.375-inch (0.95-cm) outside diameter by 0.015-inch (0.38-cm) wall.

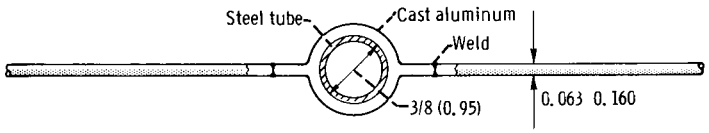

(d) Sample D. Aluminum material cast around stainless-steel tube with stub fins protruding about 0.25 inch (0.635 cm) away from aluminum tube section. Aluminum fins (3003 Al) welded to protruding stub fins. AISI 316 stainless-steel tube dimensions, 0.375-inch (0.95-cm) outside diameter by 0.015-inch (0.038-cm) wall.

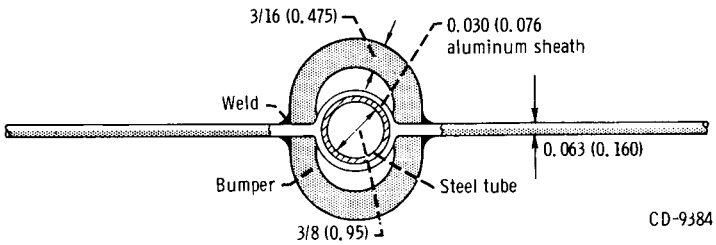

(e) Sample E. Aluminum finned-tube section machined from 1100 aluminum block. Bore of section reamed to light press fit with stainless-steel tube. Bumper sections continuously welded to produce sealed off air chamber around aluminum tube section. Ends of chambers capped off with flat pieces. AISI 316 stainless-steel tube dimensions, 0.405-inch (1.06-cm) outside diameter by 0.015-inch (0.038-cm) wall.

Figure 2. - Schematic drawings of sample finned-tube assemblies. (All dimensions, are in inches (cm).)

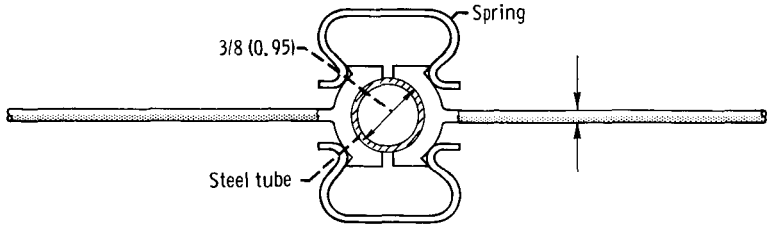

(f) Sample F. Fin halves machined from 3003 aluminum. Half fins held to stainless-steel tube by 1-inch (2.54-cm) long stainless-steel springs (three per side). AISI stainless-steel tube dimensions, 0.375-inch (0.95-cm) outside diameter by 0.015-inch (0.038-cm) wall.

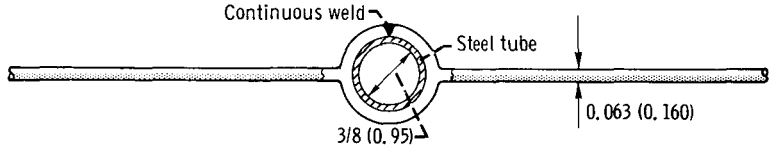

(g) Sample G. Aluminum finned-tube section machined from 1100 aluminum block. Tube section split and stainless-steel tube inserted. Aluminum tube then continuously welded in fixture that produced hoop pressure around stainless-steel tube. AISI stainless-steel tube dimensions, 0.375-inch (0.95-cm) outside diameter by 0.15-inch (0.038-cm) wall.

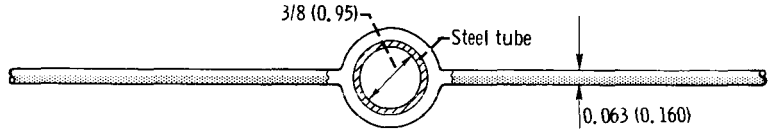

(h) Sample H. Aluminum finned-tube section machined from 1100 aluminum block. Bore of tube section reamed to diameter to produce shrink fit with stainless-steel tube. Fin heated to approximately 1000° F (811° K) to expand the bore section and then stainless-steel tube inserted. After cooling to room temperature, shrink-fit condition existed between stainless-steel tube and aluminum finned-tube section. AISI 316 stainless-steel tube dimensions, 0.405-inch (1.06-cm) outside diameter by 0.15-inch (0.38-cm) wall.

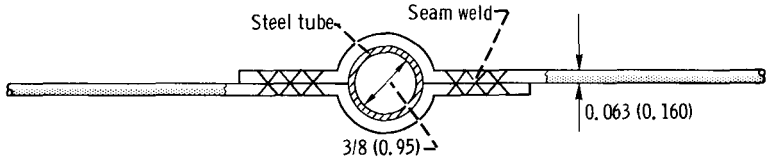

(i) Sample I. Fin halves stamped from 1100 aluminum. Circular tube section stamped to diameter 0.003- to 0.005-inch (0.007- to 0.012-cm) under stainless-steel tube diameter to ensure tight assembly when components are seam-welded together. AISI stainless-steel tube section dimensions, 0.405-inch (1.06-cm) outside diameter by 0.015-inch (0.038-cm) wall.

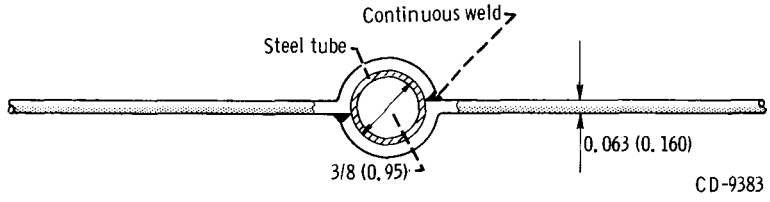

(j) Sample J. Fin halves stamped from 3003 aluminum. Continuous welded at two points. Cooling after weld produced hoop pressure on steel tube. AISI stainless-steel tube dimensions, 0.375-inch (0.95-cm) outside diameter by 0.15-inch (0.038-cm) wall.

Figure 2. - Concluded.

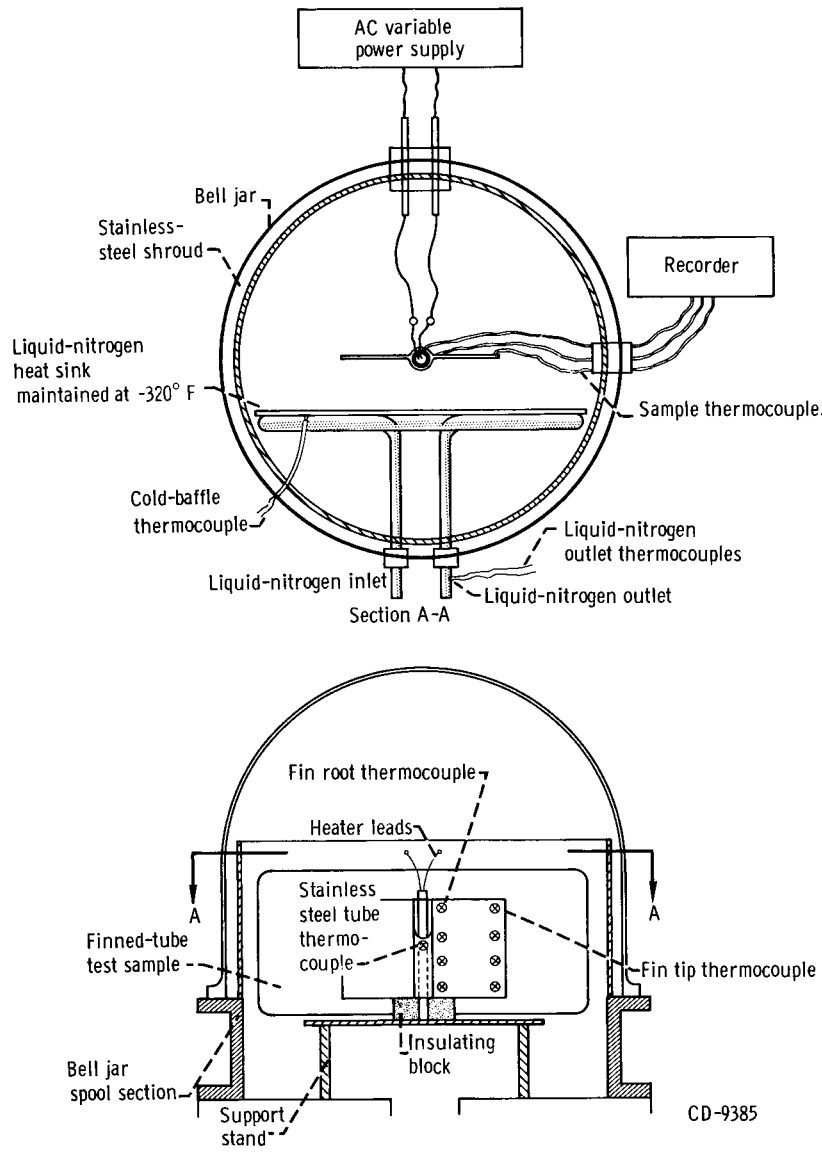

Figure 3. - Vacuum bell jar test facility.

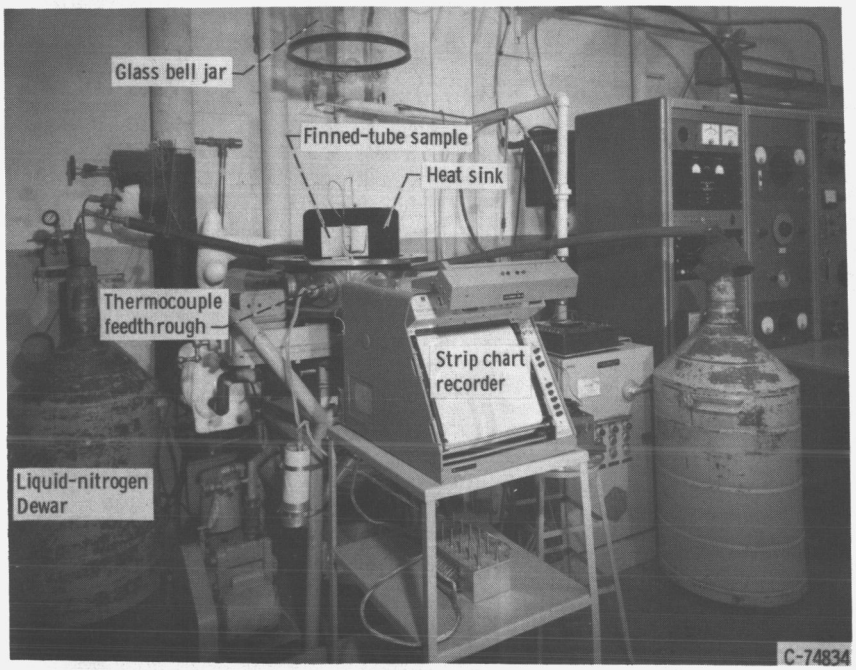

Figure 4. - Test facility showing sample.

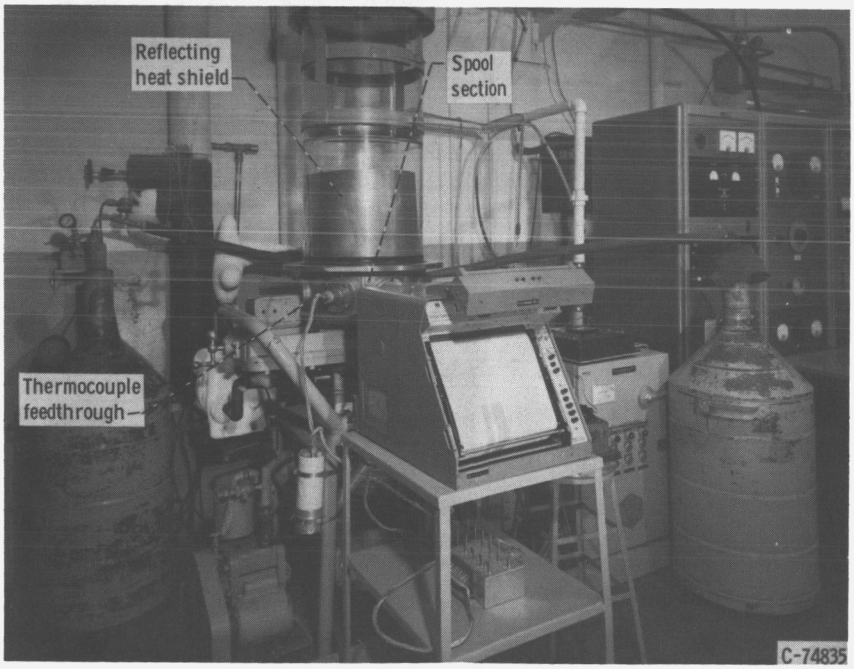

Figure 5. - Test facility showing heat shield.

heat shield was installed around the assembly and heat sink. This shield is shown installed in figure 5. The thermocouple leads and electrical connections for the heating element are brought out through insulators in the spool section under the glass enclosure.

Power (voltage) to the heating element was controlled by an autotransformer. Input power was measured by a precision wattmeter along with voltage and current. Temperatures from iron-constantan thermocouples embedded in the finned-tube assemblies and cold wall were recorded on a precision strip-chart recorder.

The finned-tube assemblies were prepared for testing in the following manner. The aluminum surfaces were sandblasted with 80-grit abrasive to give them all the same surface texture and to remove oxides. Surface roughness as measured was about 35 microinches (0.89 μm). This surface finish gave the finned-tube assemblies an average emissivity of 0.30±0.02 at ambient temperature (ref. 2). It is expected that, at the fin operating temperature range of 500° to 700° F (533° to 644° K), the emissivity would drop off 10 to 20 percent.

Nine iron-constantan thermocouples were installed on each assembly (figs. 1 and 3). Four thermocouples were embedded in the fin 0.25 inch (0.64 cm) from the edge and equally spaced. Four additional thermocouples equally spaced were embedded in the fin root next to the aluminum sheath. Because sample E had welded bumpers, the thermocouples were embedded in the fin near the bumper weld; this meant that the fin-root thermocouples were 0.25 inch (0.64 cm) away from the actual fin root when compared with the other samples. The fin-root temperature was measured so that a thermal resistance factor could be calculated for the joint and armor. In order to measure the stainless-steel-tube temperature, 0.50 inch (1.27 cm) wide section of the aluminum was machined off to expose the tube (see fig. 1). A thermocouple was then spot welded to the exposed stainless-steel tube. (On sample A this thermocouple was embedded halfway through the aluminum tube section.)

After all instrumentation was connected, the bell jar was evacuated to a pressure less than 5×10^{-5} torr (or mm Hg)(0.0066 N/m^2). Liquid nitrogen at a pressure of 3 to 4 psig (2×10^4 to 3×10^4 N/m^2 gage) was forced through the copper tubing on the heat sink. Flow was regulated so that liquid nitrogen came out of the heat skin at all times; this was to ensure that the heat sink remained at the liquid-nitrogen temperature of -320° F (78° K). When the vacuum and heat-sink temperature indicated by a thermocouple embedded in the copper-plate heat sink reached steady-state conditions, the power was applied to the finned-tube heater.

A series of tests was run in which the power to the heating element was set so that the thermocouple spot welded to the stainless-steel tube indicated 700° F (644° K). Input power in watts, voltage, and amperage were read from visual instruments. The finned-tube thermocouple outputs were recorded on a calibrated 12-channel continuously recording strip-chart recorder. Once steady-state conditions were reached, the power

was not changed for 5 minutes to see whether there would be any change in performance. Then the power to the heating element was turned off and the finned-tube assembly was allowed to cool to about room temperature. Several thermal cycles were run on each finned-tube assembly to detect any effect thermal cycling might have on the bimetallic aluminum to stainless-steel thermal resistance. The data from the last thermal cycle are used in this report. The tests of samples B to J were conducted with a constant stainless-steel tube temperature, thus eliminating as a factor the thermal resistance between the heating element and the tube. Because the finned-tube assembly lengths were not all equal, the actual power input was normalized by specifying power input per unit of tube length.

RESULTS AND DISCUSSION

Heat dissipation capability is not directly proportional to the change in bimetallic contact resistance but is a function of the sum of the aluminum, stainless steel, and bimetallic resistances. The thermal resistance from the stainless-steel tube to aluminum fins for both the metallurgical and mechanical assemblies was evaluated in two ways. The input power per unit tube length for the various finned-tube assemblies was one indication of the contact resistance at the aluminum to stainless-steel interface. The second means of indicating the thermal resistance was the ratio of the tube-to-fin temperature drop to the power input per unit tube length, as is appropriate for concentric cylinders (ref. 3).

A simplified analytical model (see fig. 6) conforming to measured temperatures was used to give a relative order of merit to the thermal contact resistance of the various finned-tube assemblies.

Because the thermocouple is spot welded on the stainless-steel tube, the temperature measured T_s is a good representation of the temperature at the stainless-steel tube surface. The overall measured temperature drop is a measure of the sum of the resistance of the aluminum and the contact resistance at the bimetallic interface of the stainless-steel and aluminum. The assumption is made that all the thermocouple junctions have the same degree of mechanical contact. The thermal conductivity of aluminum is high, 133 Btu per hour per foot per $^{\circ}$F (230.86 J/m(sec)($^{\circ}$K)) (ref. 3), at 600° F (588° K) and, conversely, its thermal resistance is low. It is assumed that the aluminum thermal resistance would not be measurably different in the various tests. Even though the aluminum temperature T_A is measured at the fin root r_3, it is also a measure of the aluminum temperature at the aluminum to stainless-steel interface due to the low thermal resistance of aluminum and the relatively short distance (0.10 in. or 0.254 cm) at the point of measurement from the interface.

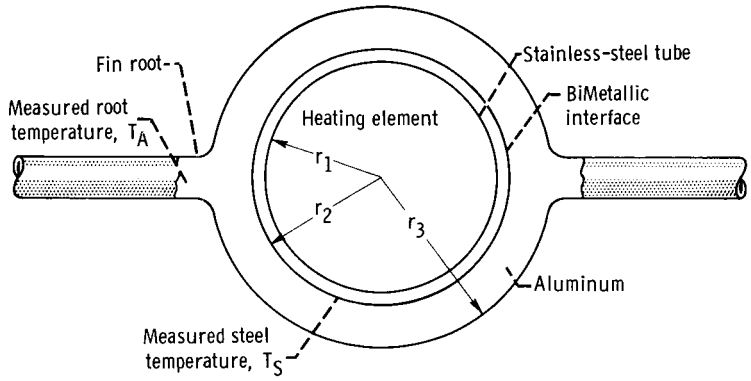

Figure 6. - Finned-tube model.

The heat flow through a substance is proportional to the temperature drop through the substance and inversely proportional to its thermal resistance. This proportionality and the previous assumptions lead to the following expression for a calculated thermal resistance factor R from measured temperatures for the finned-tube assemblies.

$$R = \frac{T_s - T_A}{Q} \frac{(^{o}F)(ft)}{Watt} \qquad R = \frac{T_s - T_A}{Q} \frac{(^{o}K)(m)}{Watt}$$

Q is the rate of heat flow (W/ft or W/m of finned-tube assembly length). This thermal resistance factor is dependent on the type of aluminum to stainless-steel joint, that is, metallurgical or mechanical. It is also dependent on the surface condition, oxidation (ref. 4), and the contact pressure (ref. 5) or lack of it.

Test data are listed in table I. In general, the metallurgically joined finned assembies had a higher heat-rejection capability than the mechanically joined assemblies. For a constant tube temperature of 700^{o} F (644^{o} K), the heat rejected by the metallurgically joined assemblies (samples B to D) ranged from 287 to 231 watts per lineal foot (941 to 758 W/m) of tube length, and for the mechanically joined assemblies (samples E to J), the rejected heat ranged from 236 to 125 watts per lineal foot (774 to 410 W/m).

The all-aluminum reference sample A (fig. 2A) had the highest heat rejection of 298 watts per lineal foot (977 W/m) (table I), as expected. Tube to fin-root temperature drop was 11^{o} F (6^{o} K), and thermal resistance factor R was 0.037 (^{o}F) (ft)/W (0.0061 (^{o}K) (m)/W).

Sample B (fig. 2), the one-piece stamping brazed to the stainless-steel tube, had the next best heat-dissipating capability, namely, 287 watts per foot (941 W/m) of tube length. Its performance was consistent and not affected by thermal cycling. One reason for this sample's high heat rejection may be the the very generous fillets of braze material. The temperature drop from the stainless-steel tube to the fin root was 21^{o} F

TABLE I. - HEAT REJECTION CHARACTERISTICS OF FINNED-TUBE ASSEMBLIES

Assembly	Construction	Input power rejected per unit of finned-tube assembly length		Stainless-steel tube temperature		Average aluminum fin-root temperature		Average fin-tip temperature		Measured thermal resistance		Thermal cycling change
		W/ft	W/m	^{o}F	^{o}K	^{o}F	^{o}K	^{o}F	^{o}K	(^{o}F)(ft)/W	(^{o}K)(m)/W	
A (reference)	Machined; all aluminum	298	977	[a]700	[a]644	689	638	618	599	0.037	0.0061	No
B	Brazed; one-piece stamping	287	941	702	645	681	634	597	587	.073	.0117	
C	Brazed; two-piece stamping	252	826	702	645	669	627	583	579	.131	.0218	
D	Cast aluminum; welded sheet fins	231	758	700	644	632	606	559	566	.295	.0501	
E	Machined aluminum; pressed tube; welded bumpers	236	774	695	641	624	602	569	572	.300	.0504	
F	Machined half fins; spring pressure	218	715	702	645	621	601	573	574	.372	.0615	Yes
G	Machined; slit; TIG welded	209	685	700	644	609	594	551	562	.435	.0730	
H	Machined; heated tube inserted	164	538	702	645	554	563	514	541	.890	.1523	
I	Formed sheet; 3/4-in. (1.9-cm) fins; seam welded	150	492	700	644	542	556	507	537	1.050	.1786	
J	Formed sheet; half fins; TIG welded	125	410	700	644	509	538	471	517	1.520	.2585	

[a]Aluminum tube section temperature, 700^{o} F (644^{o} K).

(11° K), which resulted in a calculated thermal resistance factor R of 0.073° (F) (ft)/W (0.0117° (K)(m)/W).

Sample C (fig. 2(c)), fabricated from two symmetrical half-fins brazed to the stainless-steel tube, had the third highest thermal-power-dissipating capability of 252 watts per foot (826 W/m). This dissipation capacity was about 10 percent less than for sample B and was also not affected by thermal cycling. The temperature drop from the stainless-steel tube to the fin root was 33° F (18° K), and the resistance factor R was 0.131 ($^{\circ}$F) (ft)/W (0.0218 ($^{\circ}$K)(m)/W). This finned-tube assembly had a relatively small radius (sharp transition) of aluminum sheath to fin. A pinching effect on the conductive heat flow to the fins was created, thereby causing a reduction in radiating temperature and consequently heat dissipation. Also, the stainless-steel tube had to be reamed in order to insert the heating element. In several areas the stainless-steel tube was galled by reaming thereby preventing proper contact between the heater and the steel tube.

Sample D (fig. 2(d)) had cast aluminum around the stainless-steel tube with the sheet fins welded on. It had a thermal power dissipation of 231 watts per foot (757 W/m) which was about 20 percent less than for sample B. The tube-to-fin temperature drop was 68° F (38° K), resulting in a resistance factor R of 0.295 ($^{\circ}$F) (ft)/W (0.0501 ($^{\circ}$K)(m)/W). This sample also was not affected by thermal cycling. After testing was completed on this sample, the cast aluminum was examined and it appeared to be somewhat porous. This porosity would increase the thermal resistance of the aluminum and would thereby reduce the overall heat conduction and consequently the power dissipation.

Sample E (fig. 2(e)) was somewhat different from the other finned-tube assemblies in that it had additional bumper sections welded on the fins around the cylindrical section. This was the first of the mechanical assemblies, since the stainless-steel tube was pressed into a machined one-piece aluminum sheath and fins. The bumpers (additional cylindrical tubular aluminum sections welded on) serve a twofold purpose. First, in a space environment these bumpers would protect the stainless-steel fluid-conveying tube from micrometeoroid penetration. Secondly, the bumpers affect the heat transfer in the following way. When the bumper ends were welded, a sealed chamber at atmospheric pressure was created. When the assembly was operated at a stainless-steel tube temperature of 700° F (644° K) the chamber pressure increased to 32.8 psia (2.26×10^5 N/m^2 abs). This increased-chamber-pressure increased the aluminum-sheath compressive pressure on the steel tube. Since at 700° F (644° K) aluminum is in its annealing temperature range (ref. 6), the ductile aluminum compressed on the stainless-steel tube and increased the contact pressure, thereby reducing the contact resistance. Reference 5 states that a bimetallic interface conductance increases with pressure up to around 100 psi (6.89×10^5 N/m^2) and then levels off. It might be desirable to optimize the air chamber to give the minimum pressure required to maximize bimetallic interface conductance. In the fabrication of this assembly, the bimetallic interface must be an-

nealed at 750° F (672° K) to ensure interfacial contact on subsequent heatings. During the first thermal cycle, the heat rejected was 225 watts per foot (738 W/m) of tube length. After the first cycle, the heat rejected was 236 watts per foot (774 W/m), and the stainless-steel tube to aluminum fin temperature drop was 71° F (39° K). The thermocouples that were measuring fin temperature were 0.25 inch (0.635 cm) from the root and consequently indicated a slightly lower fin temperature than expected at the root (higher temperature drop). The-resistance factor R was 0.300 (°F) (ft)/W (0.0504 (°K)(m)/W). Because the resistance factor R is inversely proportional to the tube-to-fin temperature drop, the higher fin-root temperature would yield a somewhat lower thermal resistance.

Sample F (fig. 2(f)), which was formed by two identical half-sections clamped to the stainless-steel tube by sheet-steel springs, had a heat dissipation of 218 watts per foot (715 W/m) after the first thermal cycle, during which it had been slightly higher. Figure 2 shows how the springs holding the two half-fins together caused a compression of the aluminum against the stainless-steel tube. The contact resistance might be reduced by the use of stronger springs. At the tube operating temperature, the spring material properties have to be such that there would be no setting or relaxing of the spring force over a prolonged operating period. For this particular configuration, the thermal resistance factor was 0.372 (°F) (ft)/W (0.0615 (°K)(m)/W).

Sample G (fig. 2(g)) simulated an extrusion which was saw-slit and welded together after the steel tube was inserted. The heat dissipation was 209 watts per foot (685 W/m) on the second and succeeding thermal cycles. On the first cycle the input power was 239 watts per foot (783 W/m) because of the original shrink fit from the aluminum tube welding. During the first heating, the aluminum was annealed, and it relaxed its original compressive force on the steel tube. On cooling, the aluminum could not return to its original shrink-fit condition. This was true for all the mechanical finned-tube assemblies with the exception of sample E. The thermal resistance factor for sample G was 0.435 (°F) (ft)/W (0.0730 (°K)(m)/W) after the first thermal cycle. For the first cycle, it was 0.246 (°F) (ft)/W (0.0422 (°K)(m)/W). The first-cycle data for this sample only have also been plotted in figures 7 and 8 to show the reduction in the heat dissipation from thermal cycling.

Sample H (fig. 2(h)), a second simulated aluminum extrusion, was heated to 1000° F (811° K) and the stainless-steel tube was inserted. This method of assembly may not be practical for long tubes because of the necessity during insertion of keeping the aluminum at 1000° F (811° K) and the stainless steel at room temperature. After the assembly was thermally cycled the second time and thereafter, the heat dissipated was slightly reduced to 164 watts per foot (538 W/m) of tube length. The resistance factor R was 0.890 (°F) (ft)/W (0.152 (°K)(m)/W). The aluminum tube may have become elliptical following in-

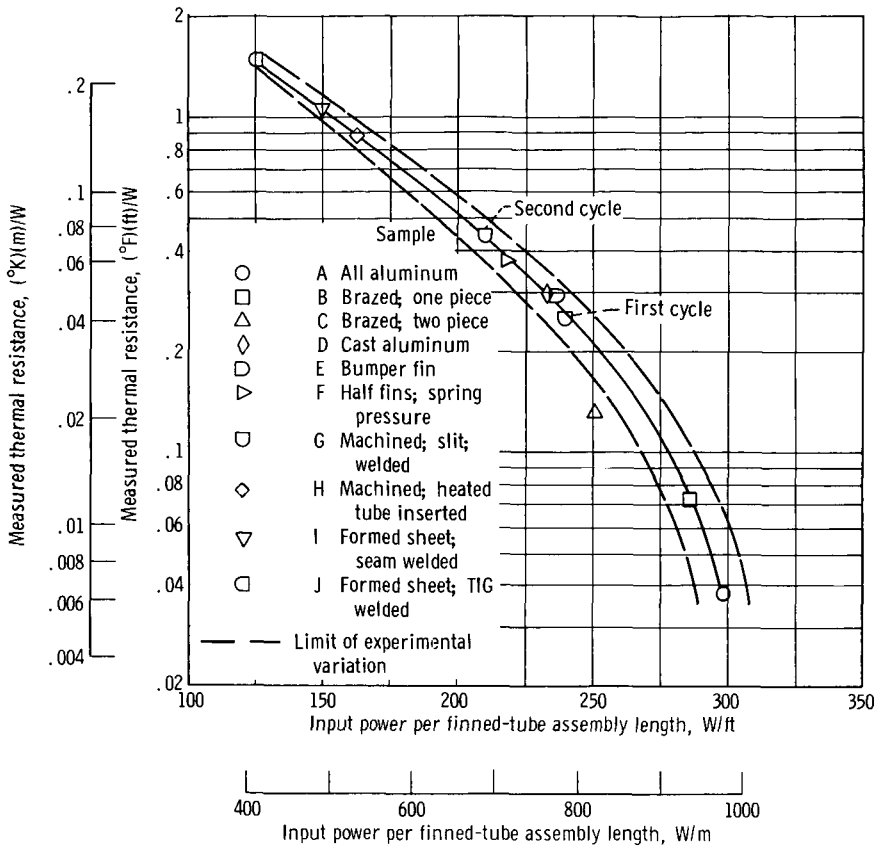

Figure 7. - Thermal resistance factor for various finned-tube assemblies. Stainless steel tube temperature, 700° F (644° K).

sertion of the stainless-steel tube because of the circumferentially uneven cooling resulting from the fins.

Sample I (fig. 2(i)) was formed from two aluminum stampings seam-welded together with the steel tube between them. The heat dissipation was 150 watts per foot (492 W/m), and the resistance factor was 1.050 (^{O}F) (ft)/W (0.1786 (^{O}K)(m)/W) after the first cycle. These values were slightly reduced from the first heating cycle, which annealed the aluminum and relaxed the hoop stress formed from the seam welding.

Sample J (fig. 2(j)) was formed from two stamped half-fins placed around the stainless-steel tube and welded together at the fin root. The heat dissipation, slightly reduced after the first thermal cycle, was 125 watts per foot (410 W/m) and the resistance factor was 1.520 (^{O}F) (ft)/W (0.2585 (^{O}K)(m)/W). After the testing was completed, this assembly was cut apart and the bimetallic interface was microscopically examined. Complete contact of the aluminum with the stainless steel was observed. It is thought that there was only slight contact pressure obtained at the bimetallic interface during fabrication.

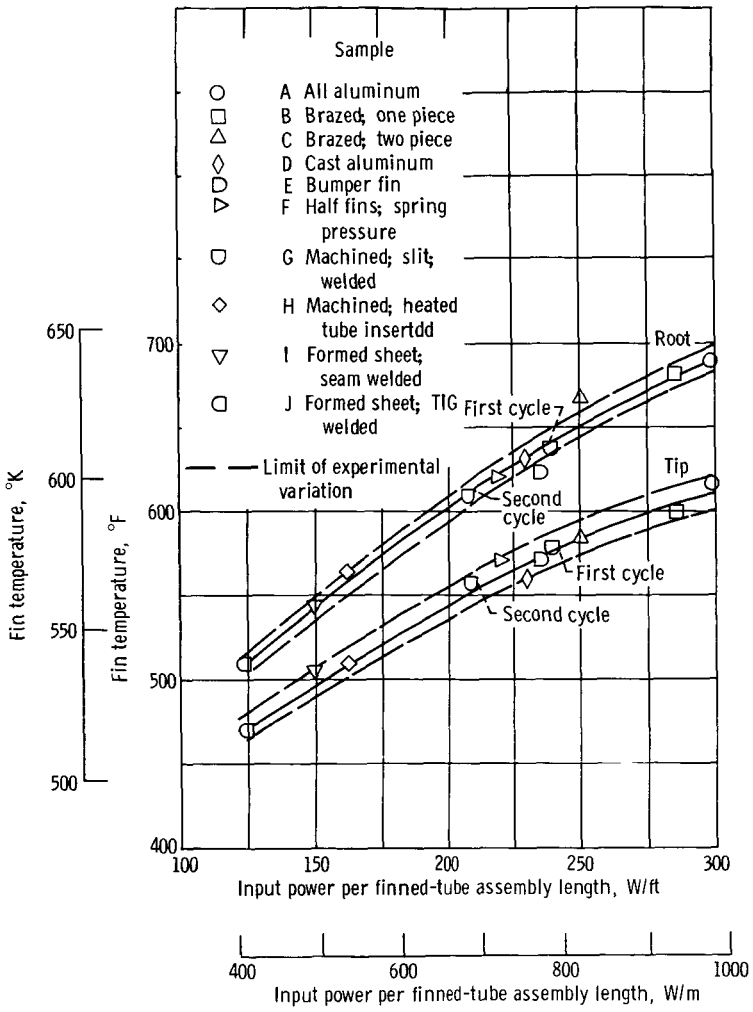

Figure 8. - Average fin temperatures at root and tip for various finned-tube assemblies. Stainless-steel tube temperature, 700° F (644° K).

Figure 7 is a plot of the measured thermal resistance factor for all the finned-tube assemblies and the all-aluminum reference sample as a function of their adjusted power input. A solid line faired through the data points shows the large variation in heat-rejection ability with thermal-resistance factor. The higher the contact resistance is, the smaller the amount of heat conducted and radiated. At the higher powers (low fin-root to tube ΔT), any experimental error of the temperature and power readings can cause an appreciable potential variation in the computed resistance factor. This experimental variation is shown as two dashed lines in figures 7 and 8. They were drawn by using the wattmeter reading accuracy of ±2 watts and temperatures that were read within $\pm 2^{\circ}$ F ($\pm 1.1^{\circ}$ K) and calibrated to within $\pm 2^{\circ}$ F (1.1° K). With the exception of sample C the data are well within the experimental variation possible. As was explained previously, difficulty was encountered on sample C in reaming the stainless steel to allow

for insertion of the heating element. It is felt that, because of an irregular contact between the stainless steel tube and the heating element, the input power was unusually low for the calculated thermal resistance factor.

Figure 8 is a plot of the average fin-root and fin-tip temperatures against input power for all the samples. These temperatures have a definite relation to thermal power dissipated for a given configuration, emissivity, and temperature level of the test. Maximum fin-root and fin-tip temperature would be when there was no bimetallic contact resistance (sample A) and the fin-root temperature was within a few degrees of the tube temperature. A solid line drawn through the data bounded by the possible experimental variations shows that, in general, the data fall within the expected variation.

CONCLUDING REMARKS

The evaluations presented in this report lead to the conclusion that the metallurgically bonded fin and tube assemblies have higher heat-rejection capability than do the mechanically bonded configurations. In addition, it is reasoned that the performance of the best heat-rejection assembly (sample B) was strongly influenced by the generous fin root to tube radii.

Fin and tube sample E, was superior in performance to all the mechanically bonded configuration investigated and also appeared to have a generous margin of material protection.

The data presented demonstrate that, when using metals such as stainless steel and aluminum, the process of shrink fitting is clearly inferior because surface contact pressure initially generated cannot be maintained after temperature cycling.

All the mechanically joined assemblies (except sample E) showed a degradation of performance after temperature cycling, some techniques more than others.

Lewis Research Center,
National Aeronautics and Space Administration,
Cleveland, Ohio, August 11, 1967,
701-04-00-02-22.

REFERENCES

1. Wintucky, William T.; Mueller, Lawrence A.; Cox, John W.; and Greenfield, Harold H.: Design and Fabrication of Noncondensing Radiator for Environmental Evaluation of Space Power Mercury Rankine System. NASA TM X-1372, 1967.

2. Merrill, Ronald; Snoddy, William; and Schocken, Klaus: The Results of Emittance Measurements Made in Relation to the Thermal Design of Explorer Spacecraft. NASA TN D-1116, 1962.

3. Kreith, Frank: Principles of Heat Transfer. International Textbook Co., 1958.

4. McAdams, William H.: Heat Transmission. Third ed., McGraw-Hill Book Co., Inc., 1954.

5. Barzelay, Martin E.; Tong, Kin Nee; and Holloway, George F.: Effect of Pressure on Thermal Conductance at Contact Joints. NACA TN 3295, 1955.

6. Anon: Alcoa Aluminum Handbook. Aluminum Co. of America, 1962.

NASA-Langley, 1968 — 3 E-3982

"The aeronautical and space activities of the United States shall be conducted so as to contribute . . . to the expansion of human knowledge of phenomena in the atmosphere and space. The Administration shall provide for the widest practicable and appropriate dissemination of information concerning its activities and the results thereof."

—NATIONAL AERONAUTICS AND SPACE ACT OF 1958

NASA SCIENTIFIC AND TECHNICAL PUBLICATIONS

TECHNICAL REPORTS: Scientific and technical information considered important, complete, and a lasting contribution to existing knowledge.

TECHNICAL NOTES: Information less broad in scope but nevertheless of importance as a contribution to existing knowledge.

TECHNICAL MEMORANDUMS: Information receiving limited distribution because of preliminary data, security classification, or other reasons.

CONTRACTOR REPORTS: Scientific and technical information generated under a NASA contract or grant and considered an important contribution to existing knowledge.

TECHNICAL TRANSLATIONS: Information published in a foreign language considered to merit NASA distribution in English.

SPECIAL PUBLICATIONS: Information derived from or of value to NASA activities. Publications include conference proceedings, monographs, data compilations, handbooks, sourcebooks, and special bibliographies.

TECHNOLOGY UTILIZATION PUBLICATIONS: Information on technology used by NASA that may be of particular interest in commercial and other non-aerospace applications. Publications include Tech Briefs, Technology Utilization Reports and Notes, and Technology Surveys.

Details on the availability of these publications may be obtained from:

SCIENTIFIC AND TECHNICAL INFORMATION DIVISION

NATIONAL AERONAUTICS AND SPACE ADMINISTRATION

Washington, D.C. 20546